

See discussions, stats, and author profiles for this publication at: <https://www.researchgate.net/publication/257837587>

Self-Assembly of Peptide-Amphiphile Forming Helical Nanofibers and in Situ Template Synthesis of Uniform Mesoporous Single Wall Silica Nanotubes

ARTICLE *in* LANGMUIR · OCTOBER 2013

Impact Factor: 4.46 · DOI: 10.1021/la4024986 · Source: PubMed

CITATIONS

14

READS

45

4 AUTHORS, INCLUDING:



Sahnawaz Ahmed

Indian Institute of Technology Guwahati

4 PUBLICATIONS 25 CITATIONS

[SEE PROFILE](#)



Julfikar Hassan Mondal

Indian Institute of Technology Guwahati

5 PUBLICATIONS 67 CITATIONS

[SEE PROFILE](#)



Debapratim Das

Indian Institute of Technology Guwahati

23 PUBLICATIONS 628 CITATIONS

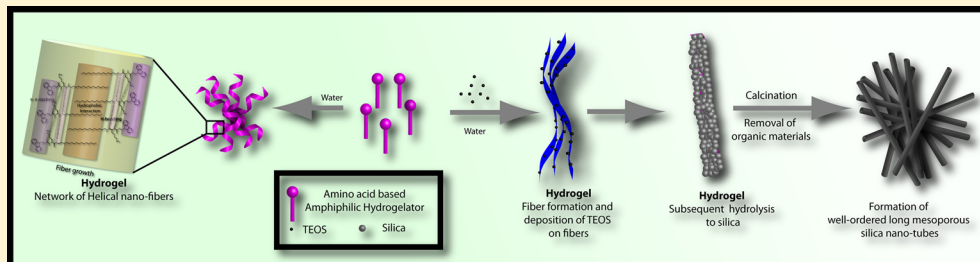
[SEE PROFILE](#)

Self-Assembly of Peptide-Amphiphile Forming Helical Nanofibers and *In Situ* Template Synthesis of Uniform Mesoporous Single Wall Silica Nanotubes

Sahnawaz Ahmed, Julfikar Hassan Mondal, Nibedita Behera, and Debapratim Das*

Department of Chemistry, Indian Institute of Technology Guwahati, North Guwahati, Kamrup, Assam 781039, India

Supporting Information



ABSTRACT: A lysine based peptide amphiphile (PA) is designed and synthesized for efficient water immobilization. The PA with a minimum gelation concentration (MGC) of 1% w/v in water shows prolonged stability and can also efficiently immobilize aqueous mixtures of some other organic solvents. The presence of a free amine induced pH dependency of the gelation as the PA could form hydrogel at a pH range of 1–8 but failed to do so above that pH. Various spectroscopic and microscopic experiments such as steady state fluorescence, NMR, IR, CD, and FESEM reveal the presence of hydrophobic interaction, hydrogen bond, and π - π stacking interaction in the self-assembly process. The self-aggregation has been correlated with the design of the molecule to show the involvement of supramolecular forces and the hierarchical pathway. While the L analogue formed left-handed helical nanofibers, the other enantiomer showed opposite helicity. Interestingly the equimolar mixture of the isomers failed to form any fibrous aggregate. Although fibers formed at a subgel concentration, no helical nature was observed at this stage. The length and thickness of the fibers increased with increase in the gelator concentration. The nanofibers formed by the gelator are used as a template to prepare mesoporous single wall silica nanotubes (SWSNTs) *in situ* in plain water without the requirement of any organic solvent as well as any external hydrolyzing agent. The SWSNTs formed are open at both ends, are few micrometers in length, and have an average diameter of ~10 nm. The BET isotherm showed a type IV hysteresis loop suggesting mesoporous nature of the nanotubes.

INTRODUCTION

The interpretations of the supramolecular assembly of small molecules have opened up the possibility to create materials of ultimate properties.^{1,2} Careful sequencing of individual constituents of a molecule allows one to prepare materials with desired material properties. Physicochemical characteristics, such as chemical functionality, rheology, morphology, as well as the stimuli sensitivity can be fine-tuned at the molecular level.^{1,2} In this regard peptide based self-assemblies come to the forefront owing to the wide range of functionalities available among the amino acids.^{3–6} Amino acid based materials not only permit one to incorporate the desired chemical functionalities but also offer the possibility of integrating biofunctionality, biocompatibility and biodegradability.³ In addition, the specific secondary, tertiary, and quaternary structures adopted by the peptide molecules provide inimitable prospects for design of nanoscale materials that are not easily available with traditional organic molecules and polymers. Owing to the aforementioned advantages, peptide based

hydrogels have attracted considerable attention of modern-day chemists and materials scientists.

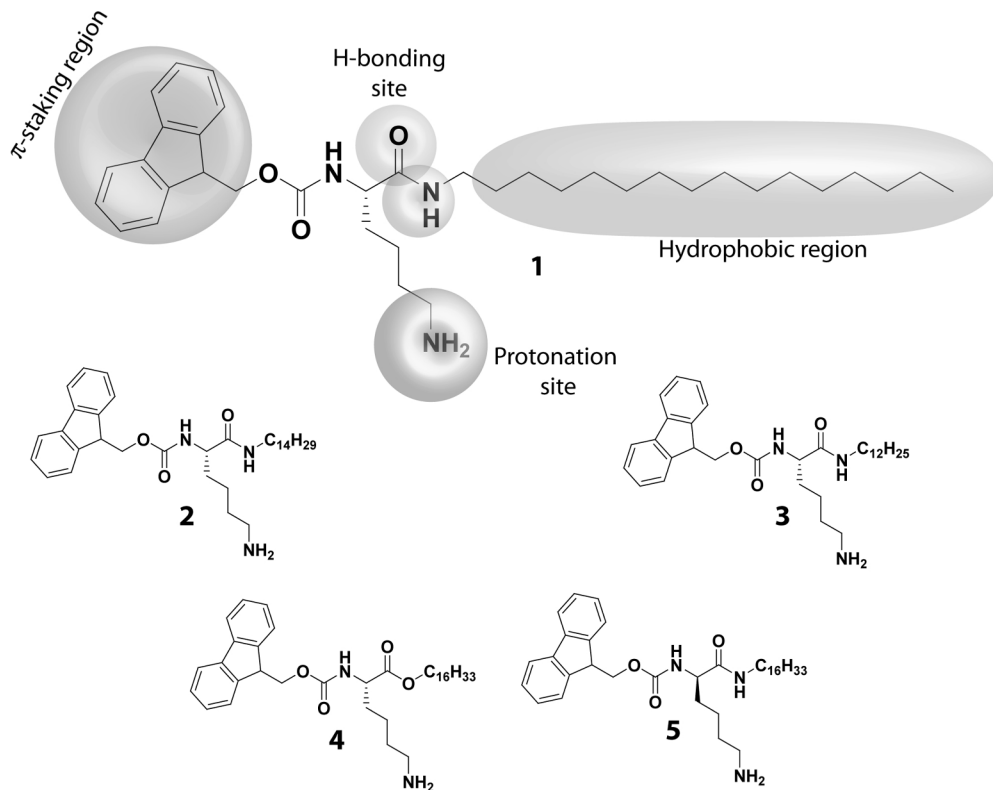
Among the peptide based hydrogelators, peptide amphiphiles (PA) are one of the major categories which demonstrate efficient self-assembly owing to the appropriate hydrophilic–lipophilic balance (HLB) within the molecular architectures.^{3,7,8} Numerous PAs have been exemplified in recent literature to show efficacious self-assembly and utilized for various applications such as tissue engineering, delivery vehicle, antibacterial agents, nanofabrication, and so forth.^{9–18} The PAs can be categorized in two major groupings: (a) amphiphilic peptides made of all amino acid and (b) lipidated peptide amphiphiles.³ Among these categories, amphiphilic peptides are more commonly found in literature as efficient hydrogelators whereas the number of lipidated peptide amphiphiles is somewhat limited. Moreover, most of these lipidated

Received: July 3, 2013

Revised: October 10, 2013

Published: October 15, 2013

Scheme 1. Structures of the Synthesized Compounds



amphiphiles are found to form supramolecular gels only in presence of some organic solvents or at a particular pH.^{9,14,15} Only a few such molecules have been reported to show hydrogelation in plain water which is essential for their biological uses.^{11,13}

The appropriate balance between all the supramolecular forces is the prime requirement for the self-assembly in a particular solvent.^{1,2} Hydrogen bonds, one key parameter controlling the assembly process, loses their strength in aqueous system while hydrophobic interaction becomes most important in such environment.^{19,20} Thus, the HLB comes into prominence while designing the lipidated peptide amphiphile as a hydrogelator. Proper HLB leads to enough solubility of the molecule to get dissolved in water and allow the other forces act in a concentration dependent fashion. The primary to tertiary assembly of a PA in water generally follows the order of micelles/bilayer-fibers and finally the gel network in a hierarchical fashion.^{1,2} The presence of chiral centers often gets transformed into supramolecular chirality in this hierarchical process.^{1–3} Peptide amphiphile based gelators thus provide interesting architectures in the nanoscale regime, and these architectures could be used as a mold for the fabrication of nanomaterials of desired shape, size and property. Indeed, a good amount of research has been reported showing the use of gelator matrix as a template for nanomaterial synthesis. These self-assembled nanofibers have been used as effective substrates for nucleation and growth of various nanoscale architectures.^{13,16,17}

To this end, nanotubes made of various materials such as carbon, gold, silver, silica, other metals, and polymers have fetched a great deal of interest because of their remarkable physicochemical properties and potential wide ranging applicability.^{21–24} Silica is one of the most studied materials

to produce nanotubes because of its inert nature, and ease of surface functionalization.^{25–28} Moreover, the mesoporous nature of such silica nanotubes make them an extremely important candidate for industrial use as catalyst support. Among the various methods available for the production of nanotubes, the template method has been proven to be versatile and inexpensive technique.²⁹ Nevertheless, template synthesis of silica relies on the organogels or alumina templates and only a few hydrogel based synthesis have been reported.^{30–32} Moreover, the hydrogel template syntheses also require an external hydrolyzing agent, an organic solvent or control over the pH of the system. In addition, maintaining uniform length and size of the silica nanotubes using hydrogel template is a difficult task and not many reports are available in literature.

Herein we describe the rational design and hydrogelation of a simple lysine containing peptide amphiphile 1 (Scheme 1) and relate the hydrogelation mechanism with the design. The PA has been found to form long helical nanofibers with relative handedness, and these fibers have been used as a template to synthesize long well-ordered mesoporous single wall silica nanotubes *in situ* utilizing the functionality available at the template surface.

MATERIALS AND METHODS

Materials. All the chemicals and solvents were purchased from Sigma-Aldrich or Spectrochem, India. ¹H NMR spectra were recorded by using an Oxford AS400 (Varian) spectrometer. ESI-MS was performed by using a Q-tof-Micro Quadrupole mass spectrophotometer (Micromass). SEM, FESEM, AFM, and TEM images were taken using LEO1430VP, SIGMA ZEISS, Agilent 5500, and JEOL JEM-2100 microscopes, respectively. Emission spectra were recorded by using an Agilent Cary-Eclipse luminescence spectrometer. CD experiments were performed by using a Jasco J-600C spectropolarim-

eter. Rheology was measured using Paar Physica Modular Compact Rheometer (MCR 301, Austria). IR spectra and DSC were recorded on Nicolet iS10 from Thermoscientific and Q-20 from TA Instruments, respectively.

Synthesis of Compounds 1–5. All the compounds were synthesized using the same synthetic protocol. Typically, 1 equiv of (L/D) Fmoc-Lys(Boc)OH was coupled with the corresponding amine or alcohol (1.2 equiv) in dichloromethane (DCM) using 1.2 equiv of HBTU, 2.4 equiv of triethylamine, and 1.2 equiv of HOBT for 24 h. The reaction mixture was then washed with brine, and the organic layer was dried over anhydrous sodium sulfate. The organic layer was filtered and concentrated on a rotatory evaporator to get the crude coupled product. It was then subjected to Boc-deprotection by trifluoroacetic acid (TFA, 4 equiv) in dry DCM. After 2 h of stirring, solvents were removed by using a rotary evaporator and the mixture was taken up in ethyl acetate (EtOAc). The EtOAc phase was washed thoroughly with aqueous 10% sodium carbonate solution followed by brine to neutrality. The organic phase was dried over anhydrous sodium sulfate and concentrated. The crude mixture was subjected to column chromatography on a 60–120 mesh silica gel column using methanol/dichloromethane as the eluent.

Characterization Data for L-(5-Amino-1-hexadecylcarbamoylpentyl)-carbamic Acid 9H-Fluoren-9-ylmethyl Ester (1). Yield: 42% (after two steps); $R_f = 0.58$ (10% MeOH in DCM); ^1H NMR (400 MHz, CDCl_3): $\delta = 0.83\text{--}0.87$ (t, $J = 7.2$ Hz, 3H), 1.23 (br, 28H), 1.37 (br, 2H), 1.59 (br, 2H), 1.81 (br, 2H), 2.95 (br, 2H), 3.20 (br, 2H), 4.12 (m, 1H), 4.42 (br, 1H), 4.66 (br, 2H), 7.28 (t, $J = 7.6$ Hz, 2H), 7.37 (t, $J = 7.6$ Hz, 2H), 7.55 (d, $J = 7.6$ Hz, 2H), 7.75 (d, $J = 7.6$ Hz, 2H) ppm; ^{13}C NMR (400 MHz, CDCl_3): $\delta = 172.21, 156.62, 143.54, 141.46, 127.45, 127.23, 127.01, 120.09, 67.35, 54.74, 54.65, 45.44, 39.64, 32.18, 31.78, 29.68\text{--}29.28$ (m), 27.12, 22.65, 22.34, 14.27; MS (ESI): m/z calcd for $\text{C}_{37}\text{H}_{57}\text{N}_3\text{O}_3$: 591.44; found 592.38 [M+H $^+$].

Characterization Data for (5-Amino-1-tetradecylcarbamoylpentyl)-carbamic Acid 9H-Fluoren-9-ylmethyl Ester (2). Yield: 43% (after two steps); $R_f = 0.54$ (10% MeOH in DCM); ^1H NMR (400 MHz, CDCl_3): $\delta = 0.83\text{--}0.86$ (t, $J = 7.2$ Hz, 3H), 1.22 (br, 24H), 1.35 (br, 2H), 1.57 (br, 2H), 1.84 (br, 2H), 2.93 (br, 2H), 3.24 (br, 2H), 4.18 (m, 1H), 4.40 (br, 1H), 4.71 (br, 2H), 7.22 (t, $J = 7.6$ Hz, 2H), 7.33 (t, $J = 7.6$ Hz, 2H), 7.51 (d, $J = 7.6$ Hz, 2H), 7.70 (d, $J = 7.6$ Hz, 2H) ppm; ^{13}C NMR (400 MHz, CDCl_3): $\delta = 172.11, 156.84, 143.56, 141.78, 127.46, 127.25, 127.11, 125.43, 67.35, 54.97, 54.66, 45.05, 39.24, 32.48, 31.65, 29.63\text{--}29.35$ (m), 27.13, 22.43, 22.24, 14.14; MS (ESI): m/z calcd for $\text{C}_{35}\text{H}_{55}\text{N}_3\text{O}_3$: 563.40; found 564.38 [M+H $^+$].

Characterization Data for (5-Amino-1-dodecylcarbamoylpentyl)-carbamic Acid 9H-Fluoren-9-ylmethyl Ester (3). Yield: 46% (after two steps); $R_f = 0.50$ (10% MeOH in DCM); ^1H NMR (400 MHz, CDCl_3): $\delta = 0.827\text{--}0.861$ (t, $J = 7.2$ Hz, 3H), 1.168 (br, 20H), 1.38 (br, 2H), 1.57 (br, 2H), 1.69 (br, 2H), 2.91 (br, 2H), 3.11 (br, 2H), 4.09 (m, 1H), 4.27 (br, 1H), 4.70 (br, 2H), 7.24 (t, $J = 7.6$ Hz, 2H), 7.33 (t, $J = 7.6$ Hz, 2H), 7.51 (d, $J = 7.6$ Hz, 2H), 7.70 (d, $J = 7.6$ Hz, 2H) ppm; ^{13}C NMR (400 MHz, CDCl_3): $\delta = 172.00, 156.88, 143.87, 141.43, 127.97, 127.29, 127.09, 120.18, 67.43, 54.66, 54.56, 45.67, 39.32, 32.01, 31.78, 29.55\text{--}29.68$ (m), 27.13, 22.88, 22.35, 14.31; MS (ESI): m/z calcd for $\text{C}_{33}\text{H}_{49}\text{N}_3\text{O}_3$: 535.37; found 536.23 [M+H $^+$].

Characterization Data for 6-Amino-2-(9H-fluoren-9-ylmethoxycarbonylamino)-hexanoic Acid Hexadecyl Ester (4). Yield: 54% (after two steps); $R_f = 0.55$ (10% MeOH in DCM); ^1H NMR (400 MHz, CDCl_3): $\delta = 0.83\text{--}0.87$ (t, $J = 7.2$ Hz, 3H), 1.18 (br, 28H), 1.36 (br, 2H), 1.56 (br, 2H), 1.73 (br, 2H), 2.94 (br, 2H), 4.05 (br, 2H), 4.09 (m, 1H), 4.27 (br, 1H), 4.70 (br, 2H), 7.24 (t, $J = 7.6$ Hz, 2H), 7.33 (t, $J = 7.6$ Hz, 2H), 7.51 (d, $J = 7.6$ Hz, 2H), 7.70 (d, $J = 7.6$ Hz, 2H) ppm; ^{13}C NMR (400 MHz, CDCl_3): $\delta = 172.00, 156.88, 143.87, 141.43, 127.97, 127.29, 127.09, 120.18, 67.43, 54.66, 54.56, 45.67, 39.32, 32.01, 31.78, 29.55\text{--}29.68$ (m), 27.13, 22.88, 22.35, 14.31; MS (ESI): m/z calcd for $\text{C}_{37}\text{H}_{56}\text{N}_3\text{O}_4$: 592.42; found 593.45 [M+H $^+$].

Characterization Data for D-(5-Amino-1-hexadecylcarbamoylpentyl)-carbamic Acid 9H-Fluoren-9-ylmethyl Ester (5). Yield: 38% (after two steps); $R_f = 0.58$ (10% MeOH in DCM); ^1H NMR (400 MHz, CDCl_3): $\delta = 0.84\text{--}0.87$ (t, $J = 7.2$ Hz, 3H), 1.21 (br, 28H), 1.36 (br, 2H), 1.57 (br, 2H), 1.81 (br, 2H), 2.95 (br, 2H), 3.20 (br, 2H),

4.12 (m, 1H), 4.42 (br, 1H), 4.66 (br, 2H), 7.27 (t, $J = 7.6$ Hz, 2H), 7.35 (t, $J = 7.6$ Hz, 2H), 7.51 (d, $J = 7.6$ Hz, 2H), 7.80 (d, $J = 7.6$ Hz, 2H) ppm; ^{13}C NMR (400 MHz, CDCl_3): $\delta = 172.21, 156.62, 143.54, 141.46, 127.45, 127.23, 127.01, 120.09, 67.35, 54.74, 54.65, 45.44, 39.64, 32.18, 31.78, 29.68\text{--}29.28$ (m), 27.12, 22.65, 22.34, 14.27; MS (ESI): m/z calcd for $\text{C}_{37}\text{H}_{57}\text{N}_3\text{O}_3$: 591.44; found 592.38 [M+H $^+$].

Preparation of the Hydrogel. In a typical experiment, 10 mg of **1** was dissolved in 1 mL of HPLC grade water by slow heating to 60 °C in a glass vial with i.d. of 10 mm. The vial was allowed to cool to room temperature without any disturbance. After three hours, an opaque gel was obtained which did not flow downward upon inversion of the glass vial.

Determination of Sol–Gel Transition Temperature (T_g). T_g was determined using vial inversion method. Typically a capped glass vial with i.d. of 10 mm containing the hydrogel was placed in a thermocontrolled oil bath and the temperature was increased at 1 °C min $^{-1}$ rate. The free flow of the hydrogel was checked by inverting the vial. The temperature at which the gel started flowing down upon inversion was noted. Here, T_g is defined as the temperature (± 0.5 °C) at which the hydrogel melts and begins to flow out of the vial. The experiments were performed in duplicate. The T_g of the hydrogel of **1** (1% w/v) was also determined using differential scanning calorimetry (DSC, TA Instruments, model Q100). Both the heating rate was 10 °C/min over 10–68 °C.

Fluorescence Spectroscopy. Fluorescence spectra of both ANS and pyrene were taken with increase in concentration of the gelator. For Pyrene, the probe was dissolved in water by overnight stirring followed by sonication for 3 h and finally filtered. All the experimental solutions were prepared by using this aqueous solution of pyrene. The fluorescence spectra of these solutions containing varying concentration of the gelator were recorded in the 350–600 nm range ($\lambda_{\text{ex}} = 337$ nm). In case of ANS, the experiments were carried out in 1:1 water-acetonitrile mixture owing to the haziness of the pure aqueous solutions at higher concentrations. As PA **1** forms efficient transparent gel in 1:1 water–acetonitrile mixture, we decided to carry out the experiments in this system. A stock (0.01 M) of ANS was prepared in the solvent mixture (1:1 water-acetonitrile) and 5 μL of the stock was added to the experimental solutions (5 mL) containing varying concentration of the gelator to reach the effective concentration of 1×10^{-5} M. The fluorescence spectra of these solutions containing varying amounts of the gelator were recorded in the 375–700 nm range ($\lambda_{\text{ex}} = 365$ nm). All the experiments were carried out at room temperature. In the case of the fluorescence of the fluorenyl group contained in the gelator molecule, the dependence of the emission spectra was determined for varying concentration of the gelator. The solutions were excited at $\lambda_{\text{ex}} = 275$ nm and the emission spectra were recorded over the range 285–510 nm. In all fluorescence experiments, emission and excitation slit widths were set at 5 and 10 nm, respectively.

Circular Dichroism (CD). The CD spectra of aqueous solutions of **1** at various concentrations were recorded by using a 1.2 mL quartz cuvette of 0.5-mm path length with a Jasco J-600C spectropolarimeter at RT. Spectra were collected at 1-nm intervals and 1-nm bandwidth from 190 to 350 nm with 1-s signal averaging time, with three-times scans for averaging. All spectra were corrected by subtracting the baseline.

Rheology. Oscillating rheology was used to quantify the final mechanical properties of the peptide amphiphile hydrogel. For the study, 2 mL of hydrogel was utilized. A 50 mm cone plate with a 1° angle configuration was used and the temperature was set constant at 25 °C. Storage (G') and loss (G'') moduli were measured at 0.1% strain with true gap 0.097 mm.

Synthesis of Silica Nanotube. In a typical experiment, 10 mg (16.92 μmol) of **1** was taken in 1 mL of HPLC grade water and the sample was heated slowly to 80 °C. It was stirred at that temperature slowly for 5 min before cooling it down to RT, and 50 μL (224 μmol) of TEOS was added to it and slowly stirred for 5 min. The mixture was then allowed to stay undisturbed for 24 h at RT for hydrolysis. The material formed gel and was transferred to a silica crucible and calcined at 550 °C for 3 h. A white solid thus obtained was utilized for further studies.

SEM, FESEM, and AFM Sample Preparation. For the hydrogel, a small portion of the gel (various concentrations) was casted on a glass plate and air-dried for 2 days before the experiments. For the silica nanotubes, the calcined material (1 mg) was dispersed in methanol (0.5 mL), and from that suspension a small drop ($\sim 100 \mu\text{L}$) was spotted on a glass plate air-dried overnight.

TEM. The silica nanotubes (1 mg) was dispersed in methanol (0.5 mL). A droplet ($\sim 20 \mu\text{L}$) of the dispersion was deposited on a clean surface. Then a copper TEM grid (300 mesh Cu grid with thick carbon film from Pacific Grid Tech, USA) was immersed into the droplet for 15 s. The excess liquid on the grid was removed with filter paper. The attached silica nanotubes on the grid were then air-dried for TEM observation.

FTIR. KBr pellets were prepared using the samples (gelator, lyophilized gel, or the silica nanotubes), and the spectra were recorded on a Nicolet iS10 spectrometer. The baseline was subtracted from the obtained absorbance intensity in each case.

N₂ Adsorption/Desorption. N₂ adsorption/desorption isotherms were obtained by using a Quantachrome Autosorb 1-C surface area analyzer at 77 K. The samples were heated at 100 °C overnight to remove all the adsorbed gases prior to the experiment. Pore size distribution was calculated employing the NLDFT (nonlocalized density functional theory) model.

RESULTS AND DISCUSSION

Recently Liu et al. have reported that Fmoc-protected glycine containing a C₁₈ chain forms organogel and twisted nanofiber like structures.³³ Based on these observations, we reasoned that decrease in the hydrophobicity and inclusion of a hydrophilic group may allow sufficient solubility to this molecule in aqueous environment. A simple lysine based amphiphile **1** (Scheme 1) was designed. A C₁₆ hydrophobic tail, functionalities capable of forming hydrogen bond (NH and carbonyl group) as well as an aromatic π-electron system in the form of fluorenyl group in the molecule would be adequate to provide enough supramolecular interactions. Appropriate solubility of the molecule is an essential criteria in order to self-organize and thus in our design, we have maintained a hydrophilic group in the form of a free amine of the lysine side chain which may allow to solubilize the molecule in water as well as keep the proper HLB to self-assemble. The presence of the free amine group is also on purpose to incorporate pH sensitivity of the self-assembly. When dissolved in plain water at 1% w/v (16.92 mM) concentration by slow heating to 60 °C, PA **1** forms a slightly hazy solution which upon slow cooling to room temperature formed a self-supporting opaque hydrogel. Based on this observation, in order to establish the hydrogelation mechanism, four structurally similar compounds were also synthesized (2–5, Scheme 1). In case of **2** and **3**, the tail lengths were varied by changing the tail to C14 and C12 respectively. Compound **4** is the ester analog of compound **1** while compound **5** was synthesized using the D-lysine isomer to get the D-analog of compound **1**.

The hydrogel was found to be stable at room temperature over a period of more than 6 months. The sol–gel transition temperature (T_g) was observed to be 47 °C which closely matched with the DSC data (see the Supporting Information). A sharp peak was observed in the forward scan of DSC indicating the T_g at 47.3 °C. In accordance with the previously reported results, the T_g increased with the increase in gelator concentration (see the Supporting Information).^{11,15} Linear viscoelastic frequency sweep response of the hydrogel of **1** (1% w/v) exhibits a weak frequency dependence from 0.2 to 100 rad s⁻¹ where G' (dynamic storage moduli) dominating G'' (loss moduli), suggesting the high elasticity of the hydrogel (see the

Supporting Information). Interestingly compound **1** also formed gel in aqueous mixtures of different organic solvents (methanol, dimethyl sulfoxide, dimethylformamide, acetonitrile, and dioxane) at 1% w/v concentration. Unlike the pure aqueous system, in all those mixed solvent systems except in methanol, the gels are observed to be transparent (see the Supporting Information).

pH Sensitivity. The presence of the free amine at lysine side chain of **1** served two purposes as it allowed the molecule to solubilize in water as well as provided the pH sensitivity of the gelation process. Compound **1** formed hydrogel in 20 mM buffers of pH 1–8 at 1% w/v concentration but failed to solubilize above pH 8. The pH sensitive aggregation could be explained based on the protonation of the free amine which remain in the ammonium state even in plain water and thus provides the solubility of the molecule in the pH range of 1–8. Above that pH, the amine group gets deprotonated which reduces its solubility at this condition. As the pH dependency was established we wanted to explore the pH responsive gelation of **1** and prepared 3% w/v hydrogel of **1** in 1 mL 20 mM buffer, pH 1 and at the top of the gel placed a 50 μL of 3 M sodiumhydroxide solution (Figure 1). After 6 hours, the gel

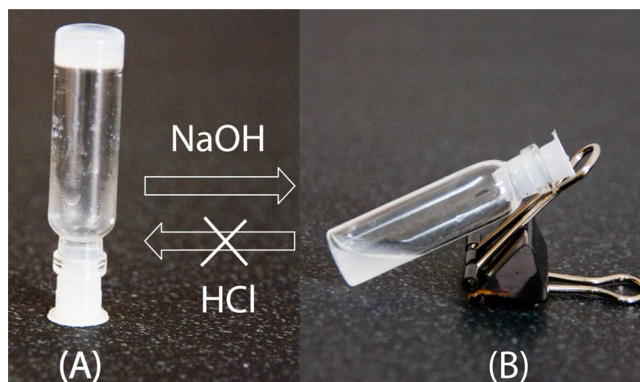


Figure 1. Photographs of pH dependent gelation of **1**: (A) Hydrogel of **1** (3% wt/vol) at pH 1 and (B) the gel transformed into a sol after addition of 3 M NaOH solution.

melted to a suspension and the pH of the system was observed to be 9. The pH of the suspension was then adjusted to 2 by adding concentrated hydrochloric acid. The acidic suspension was then heated slowly to 60 °C and allowed to come to room temperature. The suspension neither solubilized at elevated temperature nor formed a hydrogel upon cooling. The observation can be explained in terms of the removal of the “Fmoc” group under basic conditions which leads to phase separation and irreversibility of the hydrogelation process.^{34,35} Thin layer chromatography of this sample showed disappearance of the parent compound (**1**) and the appearance of another major compound with a lower retention factor along with a UV active spot at the solvent front (see the Supporting Information). The ESI-MS measurement of the material showed the mass of the deprotected product which clarifies the assumption (see the Supporting Information).

Hydrophobicity Regulates the Gelation. The peptide amphiphile **1** was designed to attain sufficient hydrophobicity which may favor the self-aggregation. In order to decipher the role of hydrophobicity in the hydrogelation process, two more analogues **2** and **3** with altered hydrophobic characters were synthesized. Although compound **2** could immobilize water to

form hydrogel at a higher concentration above 3% w/v, compound **3** failed to form any self-supporting gel in plain water. The observation was found to be similar when the experiment was repeated with a buffer of pH 1. The fall in the hydrophobic character significantly alters the HLB of the molecule and consequently the self-aggregation could not be achieved.

The presence of the hydrophobic interaction is also prominent from the emission spectra of a hydrophobic probe 8-anilino-1-naphthalenesulfonic acid (ANS) with varying concentration of the gelator (Figure 2). Due to slight haziness

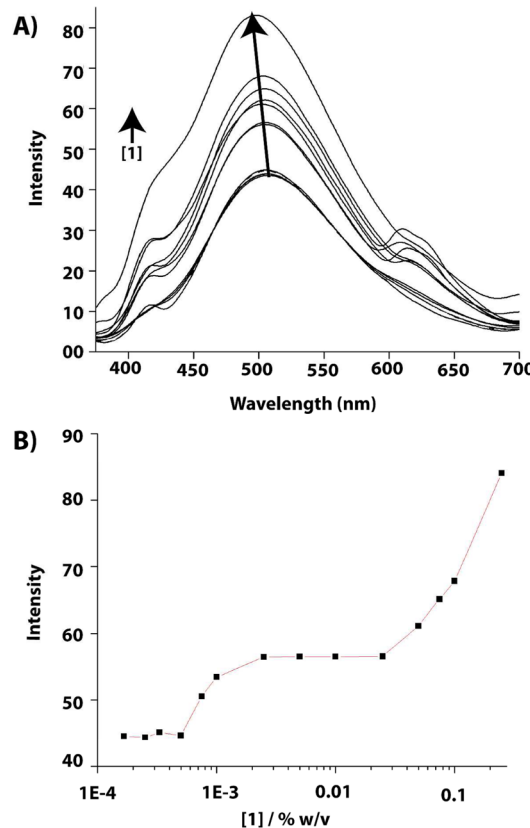


Figure 2. (A) Fluorescence spectra of ANS (1×10^{-5} M) with increasing concentration of **1** in 1:1 water acetonitrile at RT ($\lambda_{\text{ex}} = 365$ nm). (B) Dependence of fluorescence intensity of ANS on gelator concentration.

at higher concentration in aqueous medium, the experiment was performed in 1:1 water–acetonitrile medium as the gelator also forms gel in this solvent system at 1% w/v concentration. As the concentration of the gelator increased, the intensity of the emission peak showed a steady enhancement accompanied by a blue shift in the maxima from 508 to 495 nm. Such luminescence behavior of ANS indicates the existence of a hydrophobic environment.^{11,18} Moreover, the dependence of the emission intensity at 495 nm with the gelator concentration shows some interesting features. At a very low concentration below 5×10^{-4} % w/v the intensity was similar to that of only ANS in the system indicating that the gelator molecules were in monomeric form and no aggregation occurring at that concentration range. Above that concentration, the intensity increased steadily up to 2.5×10^{-3} % w/v and no further change was observed till 2.5×10^{-2} % w/v. Another inflection point was noted at this concentration. This pattern in the

intensity at this concentration range indicates two distinct self-aggregation processes happening in this concentration range. It may be presumed that the initial inflection point at 2.5×10^{-3} % w/v signifies the primary aggregation and formation of the micelles/bilayer and the second inflection point at 2.5×10^{-2} % w/v is caused by the secondary aggregation and signifies the formation of fibers at this concentration. This observation is also supported by the fluorescence experiments of the gelator alone and with pyrene as a probe where in both cases significant changes were observed at this concentration range.

Further to understand the role of hydrophobicity, the emission spectra of pyrene in the aqueous solution of **1** were recorded. The overlaid spectra in Figure 3 show an initial

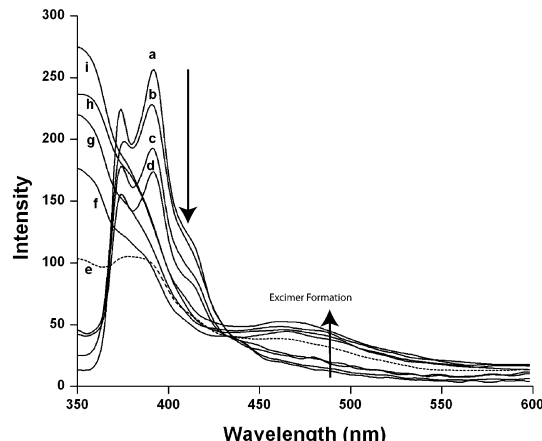


Figure 3. Luminescence spectra of pyrene (1×10^{-7} M) in aqueous solutions of various concentration of **1** at RT ($\lambda_{\text{ex}} = 337$ nm). [1] (% w/v): (a) 0.0025; (b) 0.005; (c) 0.0075; (d) 0.01; (e) 0.025; (f) 0.05; (g) 0.075; (h) 0.1; (i) 0.25.

decrease in intensity of the pyrene emission peaks with increase in concentration of the gelator. The intensity ratio (I_1/I_3) decreased with increasing concentration (data not shown) which signifies the assembly of the monomers and existence of the hydrophobic interaction in the system. Above 0.025% w/v concentration of **1**, a red-shifted peak at 470 nm appeared along with the distortion of the original fine emission structure of pyrene. The intensity of the peak at 470 nm increased with concomitant increase in the gelator concentration. This new peak at 470 nm signifies the appearance of the pyrene excimer.³⁶ With an increase in concentration of the PA, micellar aggregates were formed. Further increase in concentration probably leads to the hierarchical self-assembly process, and fiber formation started. The probe molecules may get incorporated in these fibers and hence the local concentration increases. With increase in the fiber concentration, the local concentration of pyrene molecules reached a value where they could dimerize to show the excimer band.¹¹ These data along with the chain length dependency of the gelation process clearly signifies the role of hydrophobicity in the self-assembly process.

Hydrogen Bonding. The presence of the amide NH in the molecule along with the carbonyl oxygen allows the possibility of hydrogen bonding among the gelator molecules in the self-aggregation process. To confirm the role of the amide NH, another molecule (**4**) was synthesized where the hydrogen bond donor "NH" is replaced by an ester linkage. In accord with our expectation, this analogue precipitated from the warm

solution upon cooling to room temperature even at a concentration of 0.05% w/v. The presence of the amide group facilitates the hydrogen bonding process with the neighboring molecules via NH in the case of **1**. The absence of such hydrogen bond donor in **4** makes it unsuccessful for the self-aggregation process. The involvement of the hydrogen bonds is also prominent from the IR spectra of the powder gelator and the lyophilized hydrogel. A unique NH band, centered at around 3437 cm^{-1} , was observed for solid compound **1**, which is typically involved in hydrogen bonding interactions (see the Supporting Information). In the xerogel, the peak shifted to 3395 cm^{-1} , which indicates a greater extent of hydrogen bonding interactions. The carbonyl peaks of the carbamate and the amide appeared at 1696 and 1643 cm^{-1} , respectively, in the powder gelator and both were shifted to a lower wavenumber upon gelation (1676 and 1626 cm^{-1} , respectively). The shift in the peak positions clearly points out the involvement of the hydrogen bonding by both carbonyl groups.

$\pi-\pi$ Stacking. The overlaid spectra of the temperature dependent ^1H NMR of 1% w/v **1** in D_2O shows a downfield shift of the aromatic proton signals with increase in temperature (Figure 4). At lower temperature, the system remained in the

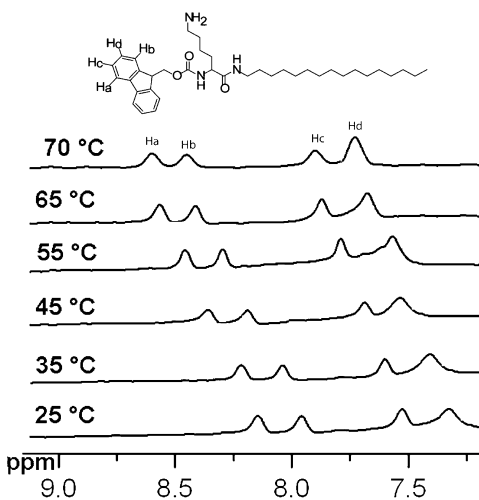


Figure 4. Temperature dependent shifts of the aromatic protons of **1** in the ^1H NMR spectra of the hydrogel of **1** in D_2O .

gel state which involves the interaction between the aromatic rings of neighboring molecules. At elevated temperature, the system gets enough heat to break the aromatic stacks and thus the protons from the π -rings shift downfield.¹¹

The presence of the stacking is further understood from the concentration dependent fluorescence spectra of the gelator (Figure 5). At a lower concentration, the emission spectra followed the pattern of Fmoc group showing two peaks at 307 and 311 nm along with a broad phosphorescence peak centered at 458 nm. Initial increase in the concentration of the gelator led to the increase in the intensity of the fluorescence peaks, whereas the phosphorescence peak diminished.^{37,38} At 0.05% w/v concentration, the well-structured emission abated and a red-shifted structure-less peak with single emission maxima at 315 nm appeared, which further red-shifted to 326 nm with an increase in concentration. Along with the red shift, another peak appeared at 425 nm. The red-shifted peak signifies the stacking of the fluorenyl groups in the system. The extra

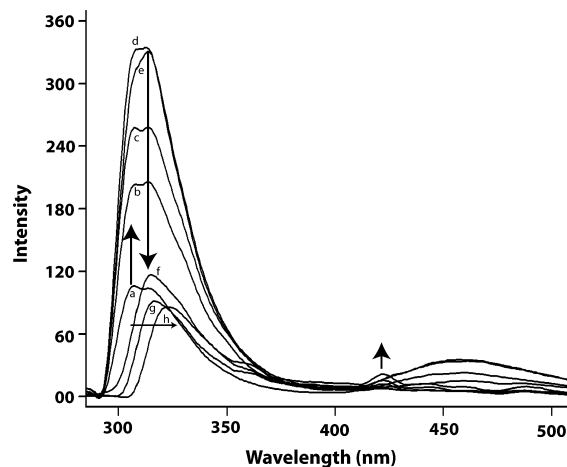


Figure 5. Fluorescence spectra of **1** in plain water at RT ($\lambda_{\text{ex}} = 265\text{ nm}$). [1] (% w/v): (a) 0.0001; (b) 0.0005; (c) 0.001; (d) 0.005; (e) 0.01; (f) 0.05; (g) 0.1; (h) 0.5.

emission band at 425 nm could be attributed to the excited dimer (excimer) emission.^{36,38} Interestingly, the red shift of the emission band started at a concentration of 0.05% w/v which is close to the concentration at which the pyrene-excimer started appearing (0.025% w/v) and could be attributed to the commencement of the hierarchical self-assembly and presumably the fibers start forming at this concentration.^{11,38}

Circular Dichroism. The concentration dependent circular dichroism spectra of **1** in water reveal some useful information on the molecular arrangement of **1** in the hydrogel (Figure 6).

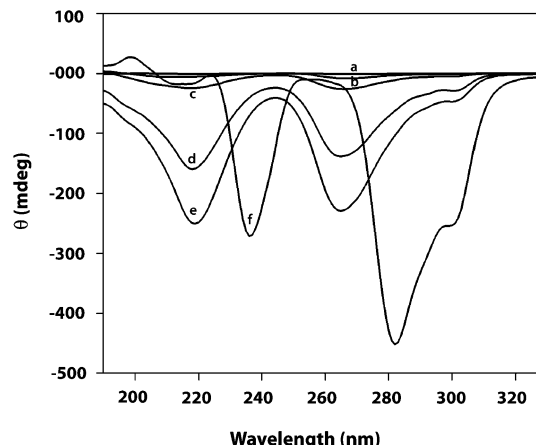


Figure 6. CD spectra of **1** in plain water at RT. [1] (% w/v): (a) 0.001; (b) 0.005; (c) 0.01; (d) 0.05; (e) 0.1; (f) 0.5.

The negative cotton effect at 220 and 264 nm indicates the superhelical arrangements of the amino acid residue which influence the helical orientation of the fluorenyl groups.^{38,39} At a higher concentration (0.5% w/v), both the bands disappear and three new bands appear at 238, 288, and 305 nm. The peaks at 288 and 305 nm are the characteristic signature of Fmoc containing gelator, but the red-shifted peak at 238 nm is unprecedented in such systems.^{38,39} A plausible explanation could be the formation of the fibers at this concentration as the final step of the overall hierarchical assembly process. This is also supported by the formation of excimer in the case of pyrene and the fluorenyl moiety around this concentration. As the network formation has started, the chirality generated by

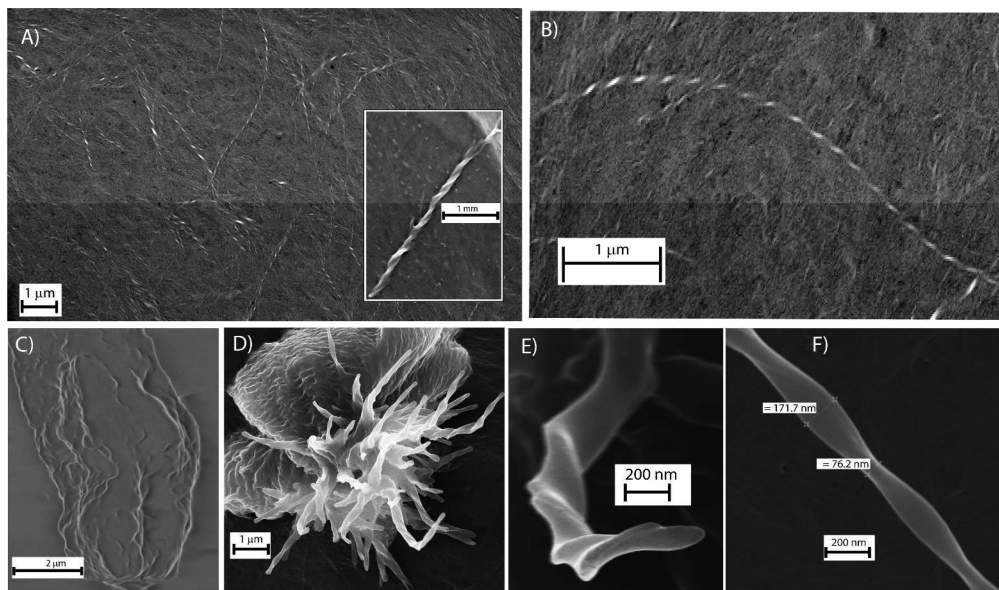


Figure 7. FESEM images of hydrogels of **1** in plain water (A) (1% w/v) showing left-handed helical fibers. Inset: right handed helical fibers obtained from hydrogel of **5** (1% w/v) in plain water. (B) Magnified view of one fiber from (A). (C) At 0.1% w/v. (D–F) At 3% w/v. (E) Closer view of one of the helical fibers showing the hierarchical overlapping of two fibers to generate a thicker fiber. (F) Closer view of one such helical fibers showing the different diameters of the fiber at different positions owing to the helical nature.

the system is now quite different than its precursor assembly. Nevertheless this phenomenon could be addressed only after detailed study in future. The CD spectra of similar experiment with **5** provided exactly the mirror images of what observed in case of compound **1** which indicates the influence of the supramolecular chirality and presence of superhelical arrangement in opposite direction in case of the D-analogue (see the Supporting Information).

Helical Fibers. The FESEM images of the dried hydrogel of **1** show network of left-handed helical nanofibers of 3–5 μm length (Figure 7). These long fibers are having a diameter of 30–40 nm. Similarly right handed helical fibers were found in case of the D-analogue **5**. Similar helical fibers were also observed in the AFM image of the hydrogel (see the Supporting Information). The helicity of the fibers is generated from the presence of the lysine residue, and as observed in the circular dichroism it induces the helical orientation at the fluorenyl moiety which subsequently gets transferred into supramolecular helicity. Interestingly, when an equimolar mixture of **1** and **5** was investigated for the gelation, no such aggregation was observed and the FESEM image of the dried sample showed no specific structural element (data not shown). The concentration dependent FESEM images show interesting features (Figure 7C–F). At a subgel concentration (0.1% w/v), thin fibers were observed but no helical nature was detected (Figure 7C). When the concentration was increased to 3% w/v, the fibers were much thicker than that at MGC (Figure 7D). Interestingly, Figure 7E shows a probable overlap of two thinner fibers which depicts the hierarchical assembly process involved. The FESEM images of all the mixed solvent gels show different types of fibrous networks. The helical nature remains in the methanol and acetonitrile systems, whereas in the case of DMSO, DMF, and dioxane normal fibers were observed (see the Supporting Information).

Results of the spectroscopic and microscopic experiments lead to the conclusion that the PA self-assembles in water in a hierarchical fashion. The concentration dependent formation of

bilayers to fibers and finally to the fibrous network are assisted by hydrogen bonding, π - π stacking and hydrophobic interactions as expected for the designed molecule. Based on these inferences, we propose a plausible mechanism for the self-assembly of PA **1** in water (Figure 8). The helicity of the fibers is generated owing to the supramolecular helicity induced by the chiral lysine residue at the fluorenyl groups in the stacking process, and hence, with elongation of the fiber, it twists along the long axis of the fiber. The presence of opposite handed helical fibers in the hydrogels of the two enantiomers as well as

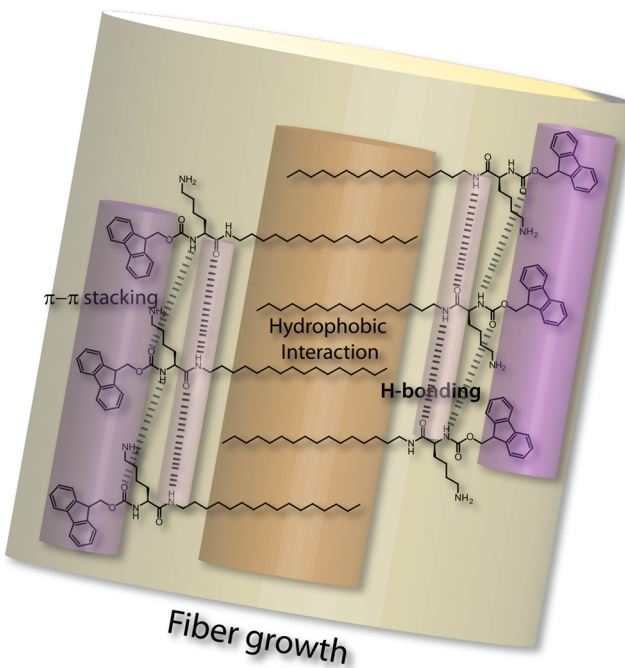


Figure 8. Schematic representation of the possible fiber formation mechanism in the hydrogel of **1**.

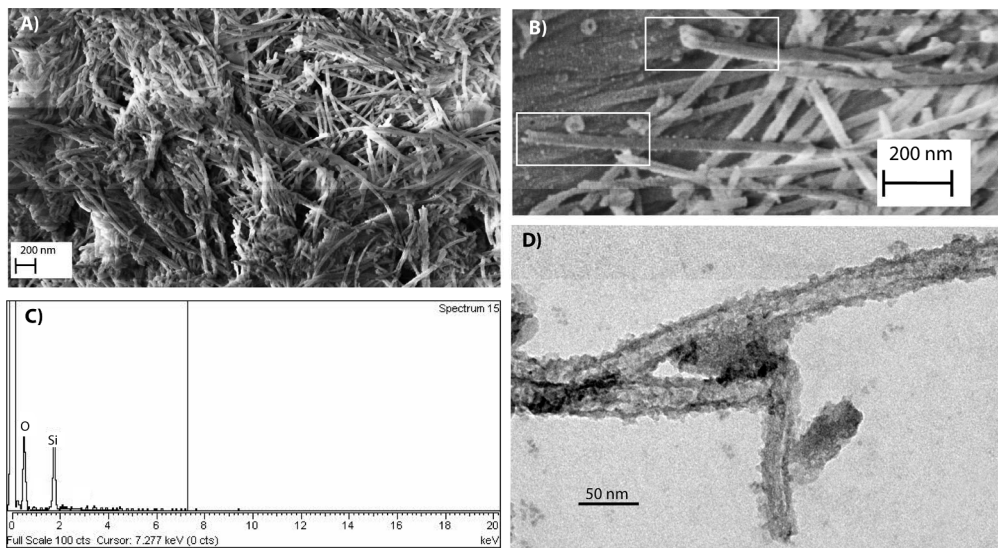


Figure 9. (A) SEM image of the silica nanotubes; (B) FESEM image of silica nanotubes showing the open end of the fibers; (C) EDX spectrum of the silica nanotubes; (D) TEM image of the silica nanotubes.

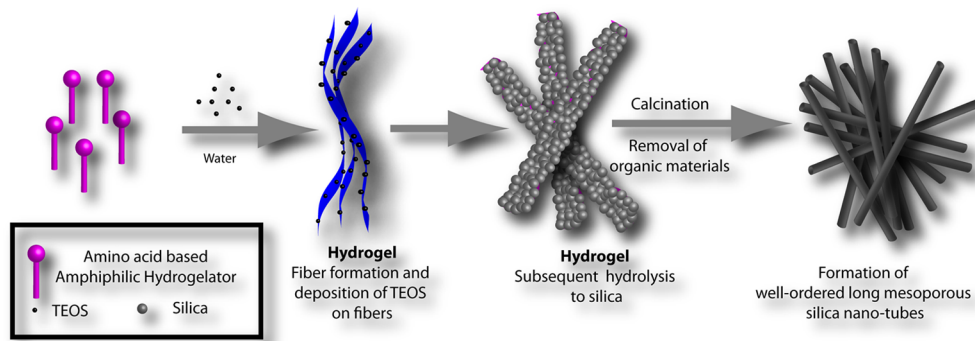


Figure 10. Pictorial presentation of the possible mechanism of silica nanotube formation.

the observation of no gelation in case of mixture of the enantiomers strongly supports this hypothesis.

In Situ Template Synthesis of Mesoporous Silica Nanotubes.

Mineralization on the nanofibers has been an area of research for a long time.⁹ The functionality available at the fiber surface allows the nucleation and growth of inorganic materials at the surface, and slow deposition leads to the formation of nano architectures of inorganic materials. We have successfully utilized this strategy to prepare mesoporous single wall silica nanotubes utilizing the nanofibers formed during the hydrogelation of PA 1. The SEM and FESEM images show extremely uniform long hollow tubes with open ends (Figure 9). The so formed silica nanotubes are more than few micrometers in length with ~10 nm inner diameter. The size closely matches with the length of the nanofibers obtained from the hydrogel of 1 at this concentration, but surprisingly the diameters are smaller than the template. To further confirm the diameter of the silica nanotubes, the TEM images of the silica nanotubes were taken. The TEM image of the nanotubes evidently shows single wall structure with uniform diameter of ~10 nm. In order to find the role of aging on the shape and size of the nanotubes, the samples were aged for 3 days before calcination, but no changes were observed in the microscopic images. The energy-dispersive X-ray (EDX) spectrum of the nanotubes clearly shows the presence of silicon and oxygen as the major constituent of the nanofibers. The IR spectra of the

silica nanotube during the synthesis shows the appearance of the Si—O—Si asymmetric band stretching at 1100 cm⁻¹ and a SiO—H stretching at 3440 cm⁻¹ along with the characteristic bands of the gelator. After calcination, all the peaks related to the gelator disappeared, leaving the characteristic bands of the silica nanotube, indicating the complete removal of the template (see the Supporting Information).

A possible mechanism of the silica nanotube formation is pictorially presented in Figure 10. When TEOS is mixed with the aqueous solution of 1, initially the gelator forms the fibers with free amines at the surface. These amine groups serve as the nucleation point, and the TEOS molecules get deposited on the fibers followed by hydrolysis by the amines. The hydrolysis and aging slowly allow the formation of the silica which coats the nanofibers. At the final step, the organic residues are removed during calcination, leaving the silica nanotubes. As the TEOS is present during the hierarchical fiber formation process, the nucleation by the free amines started at an early stage of the fibers when the thickness of the fibers was somewhat lesser than the actual fibers at this concentration (1% w/v). Thus, the helical nature could not be transformed to the silica tubes as evident from the concentration dependent FESEM study of the hydrogel which shows no helical nature of the fibers at a lower concentration (Figure 7B). This is also supported by the fact that the nature, shape, and size of the silica nanotubes were similar when the experiment was repeated at a higher gelator

concentration (3% w/v) where the thickness of the fibers is even higher than that at MGC (Figure 7D). An attempt to add TEOS after the gel formation failed, as the addition of TEOS followed by heating and subsequent cooling to room temperature did not allow the reversible formation of the fibers and hydrogel.

Porosity of the Silica Nanotubes. The specific surface areas and pore size distributions of the SWSNT are measured by nitrogen adsorption and desorption measurements. The N₂ adsorption–desorption isotherms of the silica nanotubes can be classified into type IV hysteresis loop (Figure 11), indicating

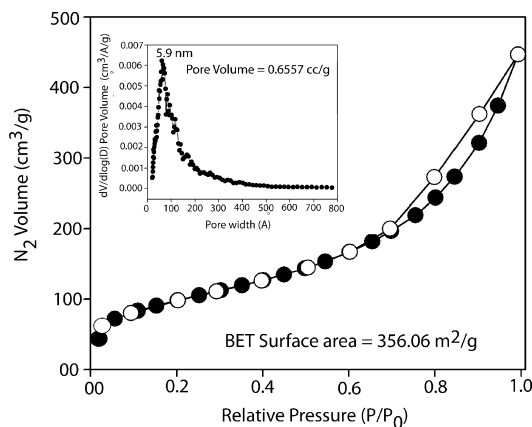


Figure 11. Nitrogen adsorption–desorption isotherms of silica nanotubes. Inset is the pore size distribution curve.

the mesoporous nature. The BET surface area calculated from N₂ adsorption/desorption isotherms is 356 m²/g, and the pore volume is determined as 0.6557 cm³/g. Although the pore size distribution curve showed a peak at 5.9 nm, the distribution is somewhat wide in nature and the range closely matches with the diameter of the nanotubes observed from microscopic images.

CONCLUSIONS

We have successfully demonstrated the rational design and hydrogelation of a simple lysine based peptide amphiphile. The hydrogelation is responsive to the change in pH, and the molecule is also able to immobilize a variety of aqueous mixtures of organic solvents. Structural elucidation of the hydrogel revealed the presence of hydrophobic interaction, π – π stacking, and H-bonding in the self-assembly process. The chirality in the molecule influenced the formation of helical nanofibers with appropriate handedness. The nanofibers are used as a template for the in situ formation of uniform mesoporous single wall silica nanotubes without the help of any external catalyst and completely in aqueous medium. Owing to the simplicity in the synthesis and the formation of well-defined helical nanofibers in plain water makes the gelator a potential candidate for various applications in nanoscience. The uniform nature of the silica nanotubes demands further analysis and holds immense promise for future applications, and study in this direction is currently under progress.

ASSOCIATED CONTENT

Supporting Information

DSC, T_g vs concentration curve, rheology, IR spectra. FESEM and AFM images and photographs of the gels formed by **1** in various aqueous mixtures of organic solvents as well as CD

spectra of compound **5**. This material is available free of charge via the Internet at <http://pubs.acs.org>

AUTHOR INFORMATION

Corresponding Author

*Email: ddas@iitg.ernet.in. Fax: (+) 91 361 258 2349.

Notes

The authors declare no competing financial interest.

ACKNOWLEDGMENTS

The authors are thankful to Prof. P. K. Das, Dr. R. R. Bhattacharjee, Ms. S. Brahmachari and Mr. S. K. Mandal for their help with various instruments. D.D. is thankful to the Department of Science and Technology, Government of India for financial assistance through fast track project and Alexander von Humboldt Foundation, Germany for instrument grant. This paper is dedicated to Swami Nityananda Maharaj.

REFERENCES

- (1) Estroff, L. A.; Hamilton, A. D. Water gelation by small organic molecules. *Chem. Rev.* **2004**, *104*, 1201–1217.
- (2) *Molecular gels: Materials with self-assembled fibrillar Networks*; Weiss, R. G., Terech, P., Eds.; Springer-Verlag: Dordrecht, 2006.
- (3) Dasgupta, A.; Mondal, J. H.; Das, D. Peptide hydrogels. *RSC Adv.* **2013**, *3*, 9117–9149.
- (4) Jonker, A. M.; Löwik, D. W. P. M.; Van Hest, J. C. M. Peptide- and protein-based hydrogels. *Chem. Mater.* **2012**, *24*, 759–773.
- (5) Gao, Y.; Zhao, F.; Wang, Q.; Zhang, Y.; Xu, B. Small peptide nanofibers as the matrices of molecular hydrogels for mimicking enzymes and enhancing the activity of enzymes. *Chem. Soc. Rev.* **2010**, *39*, 3325–3433.
- (6) Zelzer, M.; Ulijn, R. V. Next-generation peptide nanomaterials: molecular networks, interfaces and supramolecular functionality. *Chem. Soc. Rev.* **2010**, *39*, 3351–3357.
- (7) Zhao, X.; Pan, F.; Xu, H.; Yaseen, M.; Shan, H.; Hauser, C. A. E.; Zhang, S.; Lu, J. R. Molecular self-assembly and applications of designer peptide amphiphiles. *Chem. Soc. Rev.* **2010**, *39*, 3480–3498.
- (8) Löwik, D. W. P. M.; van Hest, J. C. M. Peptide based amphiphiles. *Chem. Soc. Rev.* **2004**, *33*, 234–245.
- (9) Hatgerink, J. D.; Beniash, E.; Stupp, S. I. Self-Assembly and mineralization of peptide-amphiphile nanofibers. *Science* **2001**, *294*, 1684–1688.
- (10) Duan, P.; Qin, L.; Zhu, X.; Liu, M. Hierarchical self-assembly of amphiphilic peptide dendrons: evolution of diverse chiral nanostructures through hydrogel formation over a wide pH range. *Chem.—Eur. J.* **2011**, *17*, 6389–6395.
- (11) Das, D.; Dasgupta, A.; Roy, S.; Mitra, R. N.; Debnath, S.; Das, P. K. Water gelation of an amino acid based hydrogelator. *Chem.—Eur. J.* **2006**, *12*, 5068–5074.
- (12) Bowerman, C. J.; Nilsson, B. L. A reductive trigger for peptide self-assembly and hydrogelation. *J. Am. Chem. Soc.* **2010**, *132*, 9526–9527.
- (13) Shome, A.; Dutta, S.; Maiti, S.; Das, P. K. In situ synthesized Ag nanoparticle in self-assemblies of amino acid based amphiphilic hydrogelators: development of antibacterial soft nanocomposites. *Soft Matter* **2011**, *7*, 3011–3022.
- (14) Salick, D. A.; Kretzinger, J. K.; Pochan, D. J.; Schneider, J. P. Inherent antibacterial activity of a peptide-based β -hairpin hydrogel. *J. Am. Chem. Soc.* **2007**, *129*, 14793–14799.
- (15) Ghosh, A.; Dey, J. pH-responsive and thermoreversible hydrogels of *N*-(2-hydroxyalkyl)-L-valine amphiphiles. *Langmuir* **2009**, *25*, 8466–8472.
- (16) Mitra, R. N.; Das, P. K. In situ preparation of gold nanoparticles of varying shape in molecular hydrogel of peptide amphiphiles. *J. Phys. Chem. C* **2008**, *112*, 8159–8166.
- (17) Sone, E. D.; Stupp, S. I. Semiconductor-encapsulated peptide–amphiphile nanofibers. *J. Am. Chem. Soc.* **2004**, *126*, 12756–12757.

- (18) Suzuki, M.; Yumoto, M.; Kimura, M.; Shirai, H.; Hanabusa, K. A family of low-molecular-weight hydrogelators based on L-lysine derivatives with a positively Charged terminal group. *Chem.—Eur. J.* **2003**, *9*, 348–354.
- (19) Fenniri, H.; Mathivanan, P.; Vidale, K. L.; Sherman, D. M.; Hallenga, K.; Wood, K. V.; Stowell, J. G. Helical rosette nanotubes: design, self-assembly, and characterization. *J. Am. Chem. Soc.* **2001**, *123*, 3854–3855.
- (20) Israelachvili, J. N. *Intermolecular and Surface Forces*, 2nd ed.; Academic Press: New York, 1991.
- (21) Eder, D. Carbon nanotube–inorganic hybrids. *Chem. Rev.* **2010**, *110*, 1348–1385.
- (22) Teo, B. K.; Sun, X. H. Silicon-based low-dimensional nanomaterials and nanodevices. *Chem. Rev.* **2007**, *107*, 1454–1532.
- (23) Liu, Y.; Goebla, J.; Yin, Y. Templated synthesis of nanostructured materials. *Chem. Soc. Rev.* **2013**, *42*, 2610–2653.
- (24) Shimizu, T.; Masuda, M.; Minamikawa, H. Supramolecular nanotube architectures based on amphiphilic molecules. *Chem. Rev.* **2005**, *105*, 1401–1444.
- (25) Nan, A.; Bai, X. S.; Son, J.; Lee, S. B.; Ghandehari, H. Cellular uptake and cytotoxicity of silica nanotubes. *Nano Lett.* **2008**, *8*, 2150–2154.
- (26) Mitchell, D. T.; Lee, S. B.; Trofin, L.; Li, N.; Nevanen, T. K.; Söderlund, H.; Martin, C. R. Smart nanotubes for bioseparations and biocatalysis. *J. Am. Chem. Soc.* **2002**, *124*, 11864–11865.
- (27) Ben-Ishai, M.; Patolsky, F. Wall-selective chemical alteration of silicon nanotube molecular carriers. *J. Am. Chem. Soc.* **2011**, *133*, 1545–1552.
- (28) Chen, X.; Berger, A.; Ge, M.; Hopfe, S.; Dai, N.; Göosele, U.; Schlecht, S.; Steinhart, M. Silica nanotubes by templated thermolysis of silicon tetraacetate. *Chem. Mater.* **2011**, *23*, 3129–3131.
- (29) Martin, C. R. Nanomaterials: a membrane-based synthetic approach. *Science* **1994**, *266*, 1961–1966.
- (30) Li, D.; Qu, X.; Newton, S. M. C.; Klebba, P. E.; Mao, C. Morphology-controlled synthesis of silica nanotubes through pH- and sequence-responsive morphological change of bacterial flagellar biotemplates. *J. Mater. Chem.* **2012**, *22*, 15702–15709.
- (31) Yildirim, A.; Acar, H.; Erkal, T. S.; Bayindir, M.; Guler, M. O. Template-directed synthesis of silica nanotubes for explosive detection. *ACS Appl. Mater. Interfaces* **2011**, *3*, 4159–4164.
- (32) Jiang, J.; Wang, T.; Liu, M. Creating chirality in the inner walls of silica nanotubes through a hydrogel template: chiral transcription and chiroptical switch. *Chem. Commun.* **2010**, *46*, 7178–7180.
- (33) Cao, H.; Yuan, Q.; Zhu, X.; Zhao, Y.-P.; Liu, M. Hierarchical self-assembly of achiral amino acid derivatives into dendritic chiral nanotwists. *Langmuir* **2012**, *28*, 15410–15417.
- (34) Chang, C.-D.; Waki, M.; Ahmad, M.; Meienhofer, J.; Lundell, E. O.; Haug, J. D. Preparation and properties of *N*- α -9-fluorenylmethoxy carbonyl amino acids bearing tert.-butyl side chain protection. *Int. J. Pept. Protein Res.* **1980**, *15*, 59–66.
- (35) Harrison, J. L.; Petrie, G. M.; Noble, R. L.; Beilan, H. S.; McCurdy, S. N.; Culwell, A. R. Fmoc chemstry' synthesis, kinetics, cleavage, and deprotection of arginine-containing peptides. In *Techniques in Protein Chemistry*, Hugli, T. E., Ed.; Academic: San Diego, 1989; pp 506–516.
- (36) Froster, T. Excimers. *Angew. Chem., Int. Ed. Engl.* **1969**, *8*, 333–343.
- (37) Schulman, S. In *Fluorescence and Phosphorescence Spectroscopy: Physicochemical Principles and Practice*; Belcher, R., Freiser, H., Eds.; Pergamon Press: Oxford, 1977.
- (38) Yang, Z.; Gu, H.; Zhang, Y.; Wang, L.; Xu, B. Small molecule hydrogels based on a class of antiinflammatory agents. *Chem. Commun.* **2004**, 208–209.
- (39) Berova, N.; Nakanishi, K.; Woody, R. W. *Circular Dichroism: Principles and Applications*; Wiley-VCH: New York, 2000.